# Nightside ionosphere of Mars studied with local electron densities: A general overview and electron density depressions

F. Duru,[1] D. A. Gurnett,[1] D. D. Morgan,[1] J. D. Winningham,[2] R. A. Frahm,[2] and A. F. Nagy[3]

Received 12 May 2011; revised 8 July 2011; accepted 28 July 2011; published 19 October 2011.

[1] The radar sounder Mars Advanced Radar for Subsurface and Ionospheric Sounding (MARSIS) on the Mars Express spacecraft provides local electron densities from electron plasma oscillations. Here, we use the local electron densities to study the nightside ionosphere of Mars. In this study, in which local densities were sampled to a minimum altitude of about 275 km, we measured the maximum average densities as 1000 $cm^{-3}$ on the nightside. The electron density profiles on the nightside are highly variable. An inverse exponential relationship is observed between the electron density and the altitude. At low altitudes, the median electron density decreases with increasing solar zenith angle (SZA). However, at high altitudes no dependence on SZA is observed. Steep electron density gradients, similar to the ionopause at Venus, are also observed in 15% of the passes in the nightside ionosphere. A commonly encountered structure on the nightside is an ionospheric density depression, which is a deep trough in the electron density. Nightside density depressions are large features, with an average width of 950 km. In some cases, the depressions in MARSIS data are associated with ion flow features in the Analyzer of Space Plasma and Energetic Atoms (ASPERA-3) data. In other cases, the depressions correspond to density depletion regions. Half of the depressions are aligned with the edge of the dayside-generated photoelectrons. It is concluded that several different conditions can cause the electron density depressions.

**Citation:** Duru, F., D. A. Gurnett, D. D. Morgan, J. D. Winningham, R. A. Frahm, and A. F. Nagy (2011), Nightside ionosphere of Mars studied with local electron densities: A general overview and electron density depressions, *J. Geophys. Res.*, *116*, A10316, doi:10.1029/2011JA016835.

## 1. Introduction

[2] Although there is substantial information about the dayside ionosphere of Mars, the nightside ionosphere is not as well known. In this paper, we present a study of the nightside ionosphere of Mars by the use of local electron densities obtained from Mars Advanced Radar for Subsurface and Ionospheric Sounding (MARSIS), with an emphasis on deep nightside ionospheric density depressions. Local electron densities were investigated extensively by *Duru et al.* [2008]. At the time of that investigation, very limited nightside data (about 15 full passes) were available. This paper investigates 66 full orbits between 16 February 2010 and 19 April 2010 and provides a more complete analysis of the nightside ionosphere of Mars.

[3] Prior information on the nightside ionosphere of Mars is obtained by radio occultation measurements from the Mars 4 and 5 and Viking 1 and 2 spacecraft [*Schunk and Nagy*, 2009]. *Zhang et al.* [1990] studied the nightside of Mars up to solar zenith angles (SZA) of about 125° and found that, in more than half of the samples, electron densities were too low to be measured by radio occultation. They also stated that ion transport from the dayside and particle (mainly electron) impact are the two main sources for the nightside ionosphere at Mars. *Verigin et al.* [1991] used Phobos 2 HARP spectrometer measurements and an analytic method to calculate the ionization rates. They stated that the magnetospheric electrons can be a possible source of ionization in the nightside ionosphere of Mars. The two-stream method used by *Haider et al.* [1992] showed that electron fluxes measured by the HARP instrument cause significant electron impact ionization and excitation in the nightside. Model calculations of upper limits to the nightside ionosphere by *Fox and Brannon* [1993] showed that the maximum electron density is between $1.3 \times 10^4$ and $1.9 \times 10^4$ $cm^{-3}$. A Monte Carlo transport code was used by *Lillis et al.* [2009], who concluded that the coupled effects of the crustal magnetic field gradients and electron pitch angle distributions on electron impact ionization rates are high enough that they should be included in the modeling of the nightside ionosphere.

[1]Department of Physics and Astronomy, University of Iowa, Iowa City, Iowa, USA.
[2]Southwest Research Institute, San Antonio, Texas, USA.
[3]Department of Atmospheric, Oceanic and Space Sciences, University of Michigan, Ann Arbor, Michigan, USA.


0148-0227/11/2011JA016835

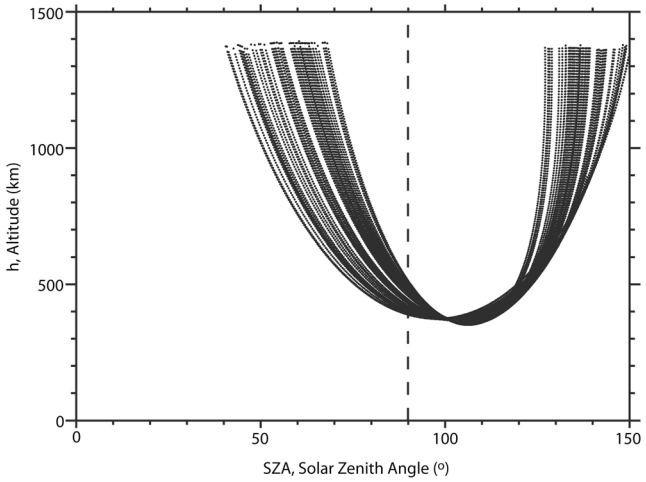


**Figure 1.** The altitude and SZA coverage of the 66 orbits analyzed in this paper. All of the passes start in the deep nightside, cross the terminator (SZA = 90°), which is marked by the dashed line, and end on the dayside.

[4] In this study we shall primarily use data from the MARSIS instrument onboard the Mars Express (MEX) spacecraft. *Safaeinili et al.* [2007], *Němec et al.* [2010], and *Němec et al.* [2011] have previously presented work on the nightside ionosphere using MARSIS data. *Safaeinili et al.* [2007] used the subsurface mode of MARSIS to calculate the total electron content of the Martian ionosphere and found that there is an enhancement in the total electron content over regions with vertical magnetic field. *Němec et al.* [2010] studied the occurrence of the nightside ionosphere through remote sounding. They reported the observed peak electron density as less than $2 \times 10^4$ cm$^{-3}$ in the majority of the cases, with peak altitudes between 100 and 150 km.

## 2. Instrumentation

[5] MARSIS, onboard MEX, is a low-frequency radar designed for subsurface and ionospheric sounding [*Chicarro et al.*, 2004]. MARSIS consists of a 40 m tip-to-tip dipole antenna, a 7 m monopole antenna, a radio transmitter, a receiver, and a digital signal-processing system [*Picardi et al.*, 2004]. A typical periapsis pass using ionospheric sounding lasts about 36 min. A quasi-sinusoidal pulse with 91.4 $\mu$s duration is transmitted at 7.86 ms intervals, stepping through 160 quasi-logarithmically spaced frequencies from 100 kHz to 5.5 MHz. The returning echoes are captured by a digital receiver with a 10.9 kHz bandwidth, which is centered on the frequency of the transmitted pulse. A complete scan takes 1.26 s and the basic sweep cycle is repeated once every 7.54 s [*Picardi et al.*, 2004]. A common way of displaying MARSIS data is with a plot of echo intensity as a function of frequency and time, called an ionogram.

[6] MARSIS performs radar soundings by transmitting a radio wave at frequency f and then by measuring the time delay of the echo reflected from the horizontally stratified ionosphere at an altitude where the wave frequency equals the electron plasma frequency [*Gurnett et al.*, 2005]. The reflection occurs because the free-space electromagnetic mode cannot propagate at frequencies below the electron plasma frequency. The electron density profile is obtained from the reflection frequency. Another way of obtaining electron densities from MARSIS is from electron plasma oscillations. When the transmitter frequency is near the local electron plasma frequency, Langmuir waves, which are strong local electrostatic plasma oscillations, are excited by the sounder pulse [*Duru et al.*, 2008]. Because of the high intensity of the electron plasma oscillations, waveforms detected by MARSIS are clipped, thereby producing harmonics. The harmonics of the oscillation frequency are seen as vertical lines equally spaced in frequency at low frequency and short delay time on an ionogram. The fundamental plasma frequency is obtained by measuring the frequency difference between two consecutive vertical lines. For a more detailed explanation see *Duru et al.* [2008]. Once the local electron plasma frequency ($f_p$) is known, the corresponding electron density ($n_e$) is calculated using $f_p = 8980\sqrt{n_e}$ [*Gurnett and Bhattacharjee*, 2005], where $f_p$ is in Hz and $n_e$ is in cm$^{-3}$. Since this method provides measurements at the location of the spacecraft, the electron densities are obtained in an altitude range between about 250 and 1300 km.

[7] This study also provides comparisons with data from the Analyzer of Space Plasma and Energetic Atoms (ASPERA-3), the plasma detector aboard MEX, which is designed to study the plasma and neutral gas environment around Mars. ASPERA-3 consists of an electron spectrometer (ELS), an ion mass analyzer (IMA), and a main unit including a neutral particle imager (NPI), a neutral particle detector (NPD), and a digital processing unit (DPU). All the parts, except for IMA, are mounted on top of a scan platform [*Barabash et al.*, 2004].

[8] The ELS is an ultralight, low-power electron top hat sensor. It has a field of view of 360° × 4° segmented into 16 sectors, each 22.5° of azimuth, with an electron energy range up to 20 keV/q [*Frahm et al.*, 2006]. The IMA contains an elevation analyzer, electrostatic top hat deflection, and an orange-section-style magnetic velocity filter. The electrostatic top hat deflection system filters energies up to 30 keV/q, providing a 360° view in 16 segments, every 22.5° of azimuth. The elevation analyzer allows a field of view of up to ±45° in 16 steps of elevation, roughly every 5.6°. Finally, the orange-section-style magnetic filter makes possible a mass spectrum up to about 40 amu [*Barabash et al.*, 2007].

## 3. General Overview

### 3.1. Data Coverage

[9] The altitude and SZA coverage of the data analyzed in this paper is shown in Figure 1. All 66 passes have trajectories that start in the deep nightside, cross the terminator (SZA = 90° marked by the dashed line), and end on the dayside. For the purpose of this study, we are interested in the region for which SZA > 90° on the right side of the terminator line as shown in Figure 1. It should be noted that the altitude coverage is not homogenous as a function of SZA. Because of the nature of the trajectories, the range covered at higher altitudes corresponds to high SZA. Lowest altitudes are about 350 km, and the spacecraft achieves SZAs of about 105°. The maximum SZA reached with these

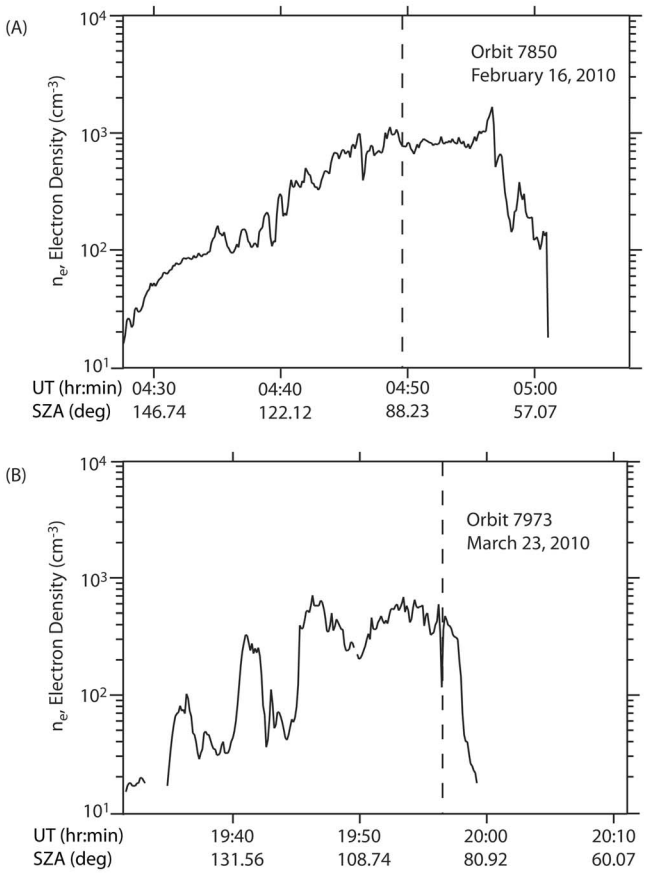


**Figure 2.** The electron density profile for two passes. The electron density is shown by the logarithmic scale on the *y* axis, and the universal time (UT) is given on the *x* axis. The dashed lines indicate the terminator, after which is the dayside ionosphere. (a) A pass from 16 February 2010 (orbit 7850). (b) A pass from 23 March 2010 (orbit 7973).

orbits is 150°. However, between 140° and 150°, the altitude coverage is only between 1100 and 1375 km.

### 3.2. Electron Density Profiles

[10] It has been previously shown that the electron density profiles of the Martian dayside ionosphere for individual orbits are highly irregular [*Duru et al.*, 2008]. We shall show from the analysis of individual passes that the nightside ionosphere is also very complex. In many orbits, complex structures, such as gaps and depressions, are present.

[11] Figure 2 provides the local electron density profile for two passes. Here, the electron density is shown by the logarithmic scale on the *y* axis, and the universal time (UT) is given on the *x* axis. The dashed lines indicate the terminator, after which the spacecraft is in the dayside ionosphere and before which the spacecraft is in the nightside ionosphere. The pass from 16 February 2010 (orbit 7850), shown in Figure 2a, is a 40 min pass that starts in the deep nightside, at a SZA of 150.32° and ends on the dayside. The electron density increases gradually with some relatively small fluctuations as the spacecraft altitude decreases. The spacecraft crosses the terminator at 0449:29 UT, and the electron density decreases after 0457:24 UT. For the last 6 min no electron density values are obtained, because no plasma oscillations can be detected. According to *Duru et al.* [2008], the disappearance of the electron plasma oscillations happen when (1) the electron density is less than 10 cm$^{-3}$, (2) the temperature is greater than about 8.5 $n_e$ °K, where $n_e$ is in cm$^{-3}$, and/or (3) the flow velocity is greater than about 160 km/s. Most of the time (as observed in this pass), the abrupt disappearance of the electron plasma oscillations occurs at high altitudes, suggesting that the spacecraft enters into the shocked solar wind, which is hot, tenuous, and rapidly flowing.

[12] The pass shown in Figure 2a has a comparatively low level of fluctuation. Most of the nightside electron density profiles have large fluctuations, such as the ones shown in Figure 2b. Here, a 40 min pass from 23 March 2010 (orbit 7973) is displayed. The electron density starts with the pass, at a SZA of 138.67° and at an altitude of 1366 km. There is a small gap in the electron density data between 1933:11 UT and 1934:41 UT. After that, the structure is very complex with high fluctuations, dips, and peaks. These types of structures are common on many nightside passes.

[13] Large density fluctuations, such as those described above, have been studied extensively by *Gurnett et al.* [2010] on the dayside of Mars. They showed that the standard deviation of the electron density decreases with increasing altitude and that there is almost no dependence on the SZA. In a similar fashion, Figure 3a provides a plot of the standard deviation of the electron density, compiled from a combination of data from all 66 orbits, calculated as half of the difference between the upper and lower quartiles, as a function of altitude in the SZA range between 90° and 150°, in 15 km altitude bins. Figure 3b shows the standard deviation divided by the median electron density, i.e., fractional standard deviation, for each altitude bin. Thus, our nightside Figure 3 is similar to the one displayed by Figure 12 of *Gurnett et al.* [2010] for the dayside. Although the actual values are much smaller for the nightside, the standard deviation of the electron density shows a similar pattern as on the dayside: it decreases as the altitude increases (around $2.5 \times 10^2$ cm$^{-3}$ at 400 km and 50 cm$^{-3}$ at 750 km). In contrast to the standard deviation, the fractional standard deviation increases as the altitude changes from 350 km to 400 km, after which it remains constant. This pattern suggests that the median electron density and the standard deviation change in comparable amounts with changing altitude.

[14] To obtain more detailed knowledge of the behavior of the electron density in the SZA range from 90° to 150°, as a function of the altitude on the nightside, electron density profiles from 66 orbits were corrected for sampling bias, meaning that the sample includes ionograms for which no plasma oscillations could be detected (it was assumed that the unmeasured plasma densities are less than 10 cm$^{-3}$), and then plotted to show the median electron density (black dots) with quartile error bars, as a function of altitude in Figure 4. More information on the minimum detectable density can be found in *Duru et al.* [2008]. The median

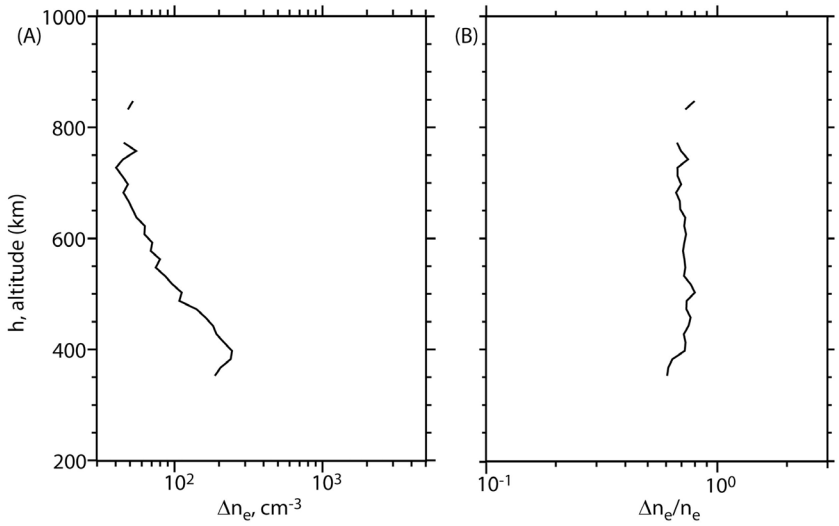


**Figure 3.** Density deviation and fractional deviation for the 66 orbits shown in Figure 1. (a) Half of the difference between the upper and lower quartiles, as a function of altitude in the SZA range between 90° and 150°, in 15 km altitude bins. (b) Half of the difference between quartiles divided by the median electron density, i.e., fractional deviation, for each altitude bin.

electron density is seen to decrease with increasing altitude. Substantial fluctuations are observed at each altitude, which can be deduced from the variations between the 25% and 75% quartiles. A slope change is observed at around 550–650 km, where the plasma environment is dominated by transport. This slope change could be caused by changing vertical/horizontal flows, or changes in temperature, temperature gradient or ion mass, which could be reflected in electron density profile. The e-folding height below and above the slope change are calculated to be around 430 km and 900 km, respectively.

[15] To study the variations of the electron density with changing SZA, plots of median electron density as a function of SZA are created for fixed altitude ranges. Shown in Figure 5, the electron density is given logarithmically on the *y* axis and SZA is shown on the common *x* axis. In order to obtain reliable statistics, we imposed the requirement of at least 5 events for each SZA bin. The error bars indicate the upper and lower quartiles for each point. It should be recalled that the altitude coverage of the data depends on the SZA, which results in restricted SZA coverage. Therefore, no solution is obtained for some SZA ranges. In the altitude range between 200 and 400 km, the median electron density decreases from about 800 cm$^{-3}$ at 95° to about 125 cm$^{-3}$ at 115°. One of the main processes responsible for the plasma on the nightside is plasma transport from the dayside [*Fox and Brannon*, 1993]. That the median electron density shows a slight decrease with increasing SZA up to 110° at low altitudes suggests that plasma transport is the main factor in this region. This result is also consistent with *Němec et al.* [2010], who studied the nightside through remote sounding data from MARSIS and concluded that the occurrence frequency of the nightside ionosphere decreases with increasing SZA up to about 125°. After 600 km, the median electron density drops below 100 cm$^{-3}$ in every SZA range and becomes more scattered. It could be assumed that median electron density is nearly constant at high altitudes, for the SZA range between 120° and 160°.

## 4. Nightside Steep Density Gradients

[16] Steep gradients in the electron density, which are the classical definition of the ionopause at Venus, have been shown to exist in the dayside ionosphere of Mars [*Duru et al.*,

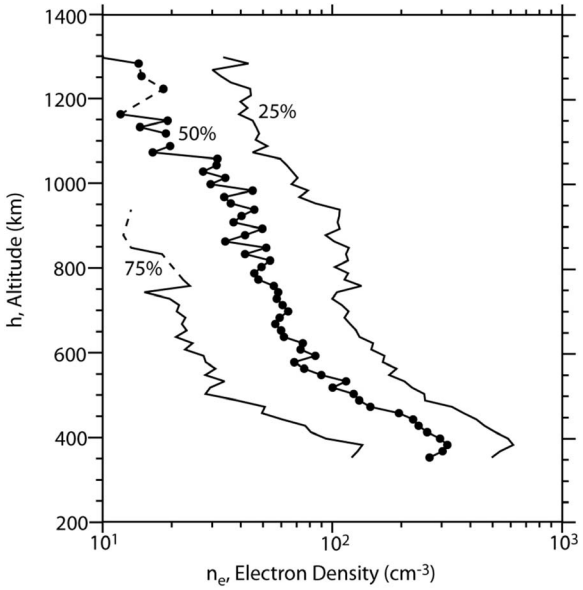


**Figure 4.** Median electron density (given by the black dots), 25% (the rightmost line) and 75% (leftmost line) quartiles as a function of the altitude, in the SZA range between 90° and 150°. This electron density profile is corrected for sampling bias, meaning that it includes ionograms for which no plasma oscillations could be detected. It is assumed that the unmeasured plasma densities are less than 10 cm$^{-3}$.

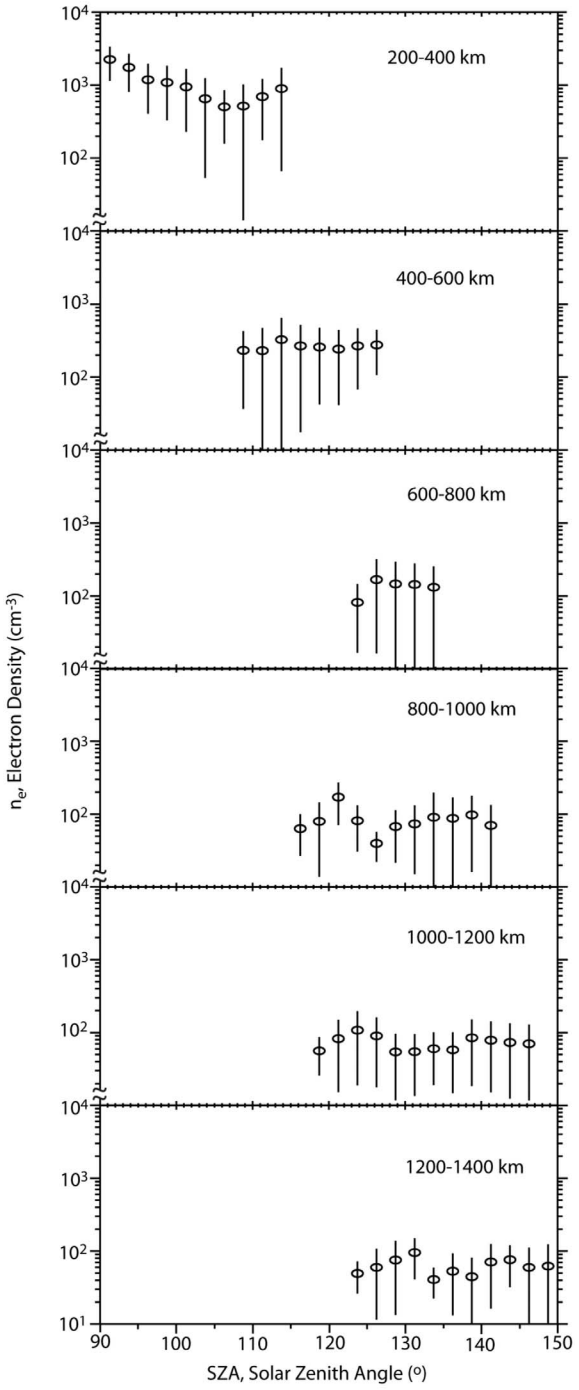


**Figure 5.** Median electron density as a function of the SZA in fixed altitude ranges. The electron density is shown on the logarithmic *y* axis, and SZA is shown on the common *x* axis. The error bars indicate the upper and lower quartiles for each point.

2009]. In contrast to Venus, steep density gradients at Mars are observed in only 18% of the samples studied, suggesting that they are transient cases. Investigation of the nightside ionosphere of Mars revealed that comparably steep density gradients occur in some of the nightside passes. An example is shown in Figure 6a that is for a nightside pass on 13 March 2010 (orbit 7937). The pass starts in the deep nightside, at a SZA of 142.90° in the Southern Hemisphere and ends on the dayside in the Northern Hemisphere. Electron plasma oscillations start at 0853:46 UT. At this point, the electron density is around 70 cm$^{-3}$ and stays in that range, with some fluctuations, until 0900:41 UT, when it starts to decrease to form a deep depression compared with the surrounding region. Then, the electron density increases back until a second depression is encountered around 0910:30 UT. The second depression ends at 0912:07 UT, and a steep density gradient is observed after this time. The local electron density increases from 22 cm$^{-3}$ to 720 cm$^{-3}$ in about a minute. This increase is not as large as those seen on the dayside of Mars, because the ionospheric densities are much lower on the nightside.

[17] In order to define the steepness of the density gradients on the nightside, the criteria used for the dayside (see *Duru et al.* [2009]) could not be applied because of the low values of the electron density. Instead, all the cases that show steeper density gradients with respect to the other nightside passes were examined to reveal that the electron density at the higher end of the gradient is greater than 150 cm$^{-3}$, and the electron density values at the lower end are lower than 30 cm$^{-3}$.

[18] Figures 6b and 6c show the ASPERA-3 ELS and IMA data, respectively. The color code in Figure 6b, gives the electron flux at each energy, and in Figure 6c, it gives the ion flux at each energy. Examining this pass more in detail, it begins on the nightside and MARSIS detects number densities less than 100 cm$^{-3}$. There is a density depletion first observed starting at about 0901:30 UT in the MARSIS number density data, reaching its minimum depression between 0902:48 UT and 0903:42 UT, and recovering to its predepression value at about 0906:20 UT. This depression occurs gradually and is not classified with steep density gradients as described above. Note that at the time of the minimum in this depression, there is almost no change in the electron flux, but the ion flux becomes less than the IMA threshold. This event occurs when the spacecraft is in total darkness.

[19] A second depression is observed in the MARSIS data between 0910:30 UT and 0912:07 UT. This density depletion is classified as having steep density gradients as described above. During this depletion, there is local sunset at the spacecraft. While in sunlight, the ELS observes a characteristic dayside ionosphere electron signature with photoelectron peaks near 20 eV observed energy (not corrected for spacecraft potential). These electrons are liberated from the photoionization of atmospheric $CO_2$ and O by He II 30.4 nm solar photon and are created on the dayside on Mars [*Frahm et al.*, 2006, 2010]. This kind of photoelectron plasma will be referred to throughout this paper as peaked photoelectron plasma (PPP). During this depression, the ion signature again shows that the flux intensity becomes less than the IMA threshold. A depression of this kind is seen in 5 of the 10 cases just before the steep density gradient. The nature of these depressions will be discussed extensively in section 5. Immediately after MARSIS observes the highest densities, there is another decrease in the electron density, as the spacecraft enters the magnetosheath on the dayside, at about 0925 UT. At the transition between ionospheric plasma and plasma from the magnetosheath, the electron data often show a boundary of finite thickness, where mixing between shocked sheath plasma and ionospheric

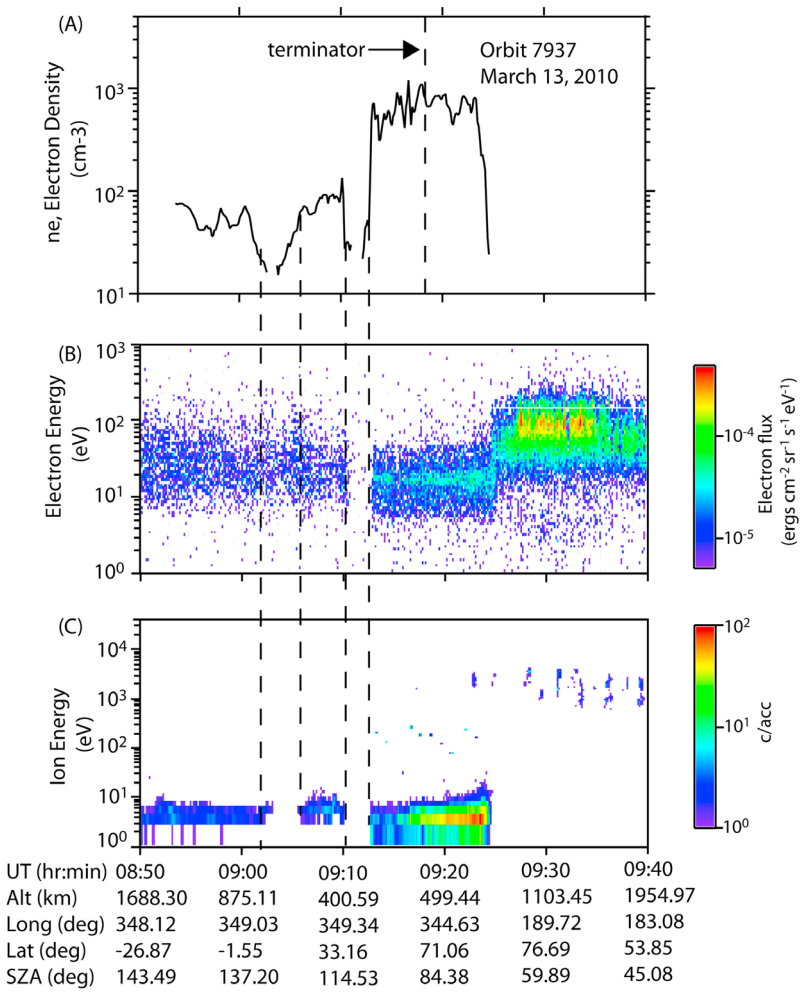


**Figure 6.** MEX data for the pass on 13 March 2010 (orbit 7937). (a) Local electron density profile from MARSIS, showing a steep electron density gradient, observed at 0912:07 UT. (b) ASPERA-3 ELS data from sector 9. The color code gives the electron flux at each energy. (c) ASPERA-3 IMA data from sector 0. The color code provides the ion flux at each energy. First electron density depression shows ion flux depletion, whereas the second depression shows both ion and electron flux depletion.

plasma occurs; the ionospheric plasma is more dominant on the ionospheric side of the boundary and magnetosheath plasma is more dominant on the magnetosheath side of the boundary. At altitudes below this transition, low-energy ion flux typically indicates planetary plasma. The ion average energy increases with altitude in the ionosphere until the higher-energy sheath plasma is observed, which is dominated by a composition reflecting the solar wind.

[20] Out of 66 orbits, only 10 passes display steep density gradients. This corresponds to about 15% of the total sample, which is consistent with the 18% occurrence rate observed by *Duru et al.* [2009] on the dayside. Therefore, as on the dayside, the nightside steep density gradients are also transient. In addition to the reasons valid on the dayside, such as instabilities due to solar wind, the lower electron density levels on the nightside would prevent the observation of a clear steep density gradient.

[21] The steep density gradient seen in Figure 6 is observed in the middle of the MARSIS pass at a SZA of 108.12°. In only two cases, the steep density gradient is observed at the beginning of the pass, at very high altitude and SZA. Figure 7 shows the SZA dependence of the altitudes of steep density gradients along with the data coverage given by the black dots. The altitude starts around 400 km for SZA around 110° and, by the altitude of about 1100 km, the SZA is around 140°. The fact that the altitude increases with increasing SZA is consistent with the statement that the steep density gradients are mostly observed at altitudes where the photoelectrons become dominant: As the SZA increases, the altitude of the boundary where PPP is observed increases. Although it is possible that the data coverage has an effect on this trend, it is observed that all the points lie on a curve and are not scattered.

## 5. Nightside Ionospheric Density Depressions

### 5.1. Observations

[22] One of the structures encountered in the nightside ionosphere of Mars is deep nightside electron density depressions, which are seen as deep troughs in the electron

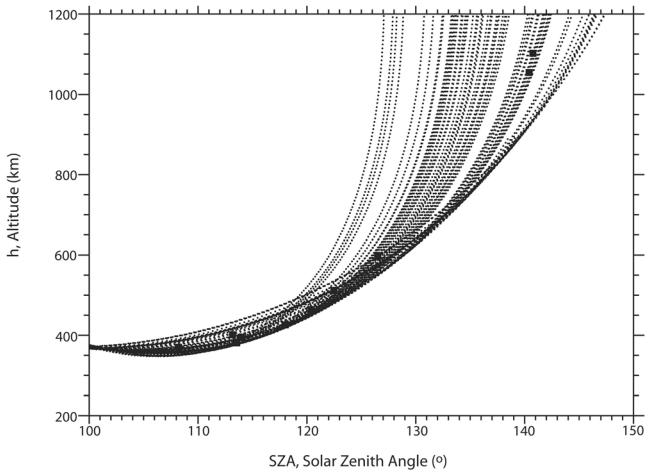


**Figure 7.** The SZA dependence of the ionopause altitudes. The gap between around 130° and 140° is due to data coverage.

density. Similar features are frequently observed in the nightside ionosphere of Venus and they are called electron density holes [*Brace et al.*, 1983], which are interpreted as crossings through plasma channels extending downstream from magnetic polar regions [*Pérez-de-Tejada*, 2001, 2004].

[23] An example of a nightside depression at Mars is shown in Figure 8a, which provides the electron density profile for a pass on 22 February 2010 (orbit 7872). The trajectory of this pass starts on the nightside and proceeds to the dayside after crossing the terminator, which is indicated by the vertical dashed line. The electron density is observed starting from the beginning of the MARSIS pass. After about 3 min the density reaches its lowest values (below the MARSIS measurement threshold), between about 1254 UT and 1306 UT. Then, the density increases (above the MARSIS density threshold) and reaches its maximum value at around 1314 UT, on the dayside after parapsis. Between 1254 UT and 1306 UT, when the depression is observed, the electron plasma oscillations observed by MARSIS disappear; and therefore, an electron density value is not obtained in that

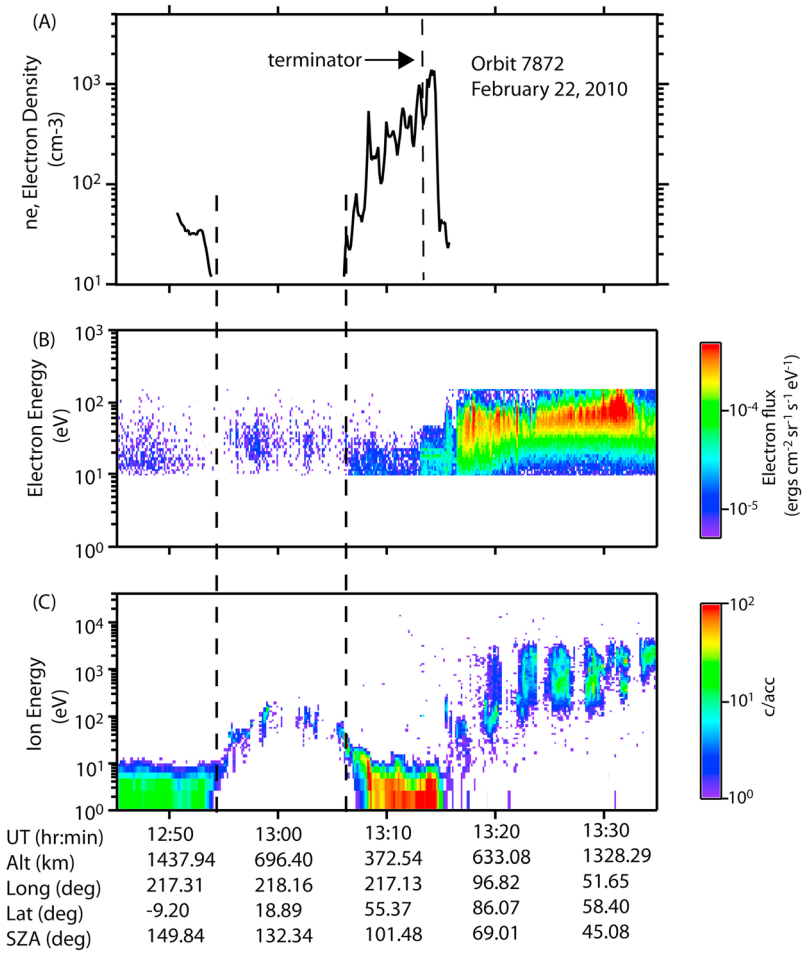


**Figure 8.** An example of a night side density depression at Mars for a pass on 22 February 2010 (orbit 7872). (a) Local electron density profile from MARSIS. The vertical dashed line indicates the terminator, after which is the dayside ionosphere. Between 1254 UT and 1306 UT, the depression is observed. (b) ASPERA-3 ELS data for sector 9. Color code shows the electron flux. (c) ASPERA-3 IMA data for sector 0, where the color code provides the flux of ions. An arch-like structure is observed where the MARSIS density depression is present, suggesting an ion flow feature.

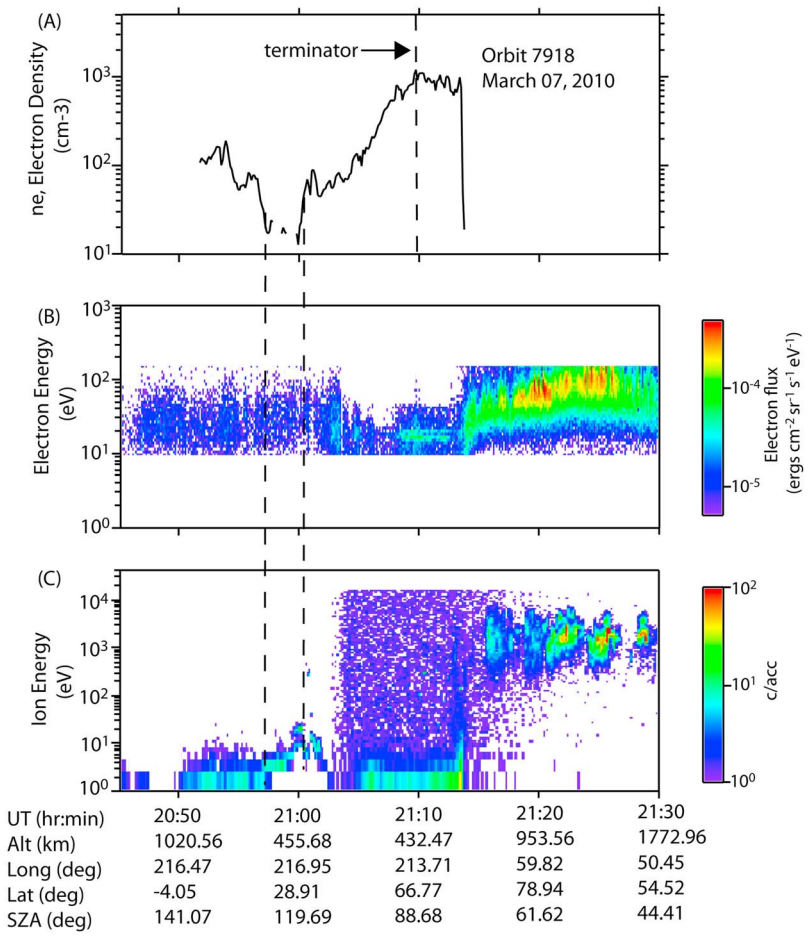


**Figure 9.** Another example of a nightside depression at Mars from the pass on 7 March 2010 (orbit 7918). (a) Electron density profile from MARSIS. Terminator is given by the vertical dashed line. The depression is observed between 2058 UT and 2059 UT. (b) ASPERA-3 ELS data from sector 9, where the color code provides the electron flux. (c) ASPERA-3 IMA data from sector 0. Ion flux is given by the color code. The electron density depression coincides with an increase in low-energy ion flux, which, this time, could be due to spacecraft charging.

period. In this pass, the trend of the density profile suggests that the electron density is below 10 $cm^{-3}$ where an interruption in the electron density is observed. Most of the density depressions (22 of 27), such as the one shown in Figure 8, show breaks in the local electron density data. For the remaining five cases, the electron density decreases to the lowest value and increases back without a break in the electron density data.

[24] The ASPERA-3 data for orbit 7872 is shown in Figures 8b and 8c in the same format as in Figure 6. In this pass, the ELS is in the fast-sweep mode, measuring over a narrower energy range, from about 9 eV to 150 eV, every 1 s. The ELS electron data show a decrease during the depression in the MARSIS data. The ion energy, seen in IMA data, drifts up and then back down over a 12 min period, forming an arch structure, peaking at about 100 eV. The data suggest that the ions are being accelerated away from the planet and escaping.

[25] The increase in the low-energy ion flux is observed in 10 of the 23 depressions for which the ASPERA-3 data are available. Both spacecraft charging and ion flow can cause this increase. The gradual arching structure in ion energy, which lasts over 5 min, typically indicates an ion flow feature, whereas ion energy changes on a very short (seconds) time scale typically indicate a charging feature. Additionally, charging features are observed to have the same energy effect on all IMA sectors, whereas flow features present different energy signatures in different IMA sectors. When a charging feature is observed on the nightside of Mars in the ion data, typically the flux intensity of the electron data is too low and its average energy is too high to allow meaningful observations of the corresponding energy shift.

[26] Another example of a nightside depression at Mars is shown in Figure 9a. This is a pass on 7 March 2010 (orbit 7918). Again, the trajectory starts on the nightside and proceeds to the dayside after crossing the terminator, indicated by the vertical dashed line. The electron density is observed starting from the beginning of the MARSIS pass. After about 4 min, the density starts to decrease and reaches its lowest values between about 2058 UT and 2059 UT. Then, it rebounds and reaches a maximum value around

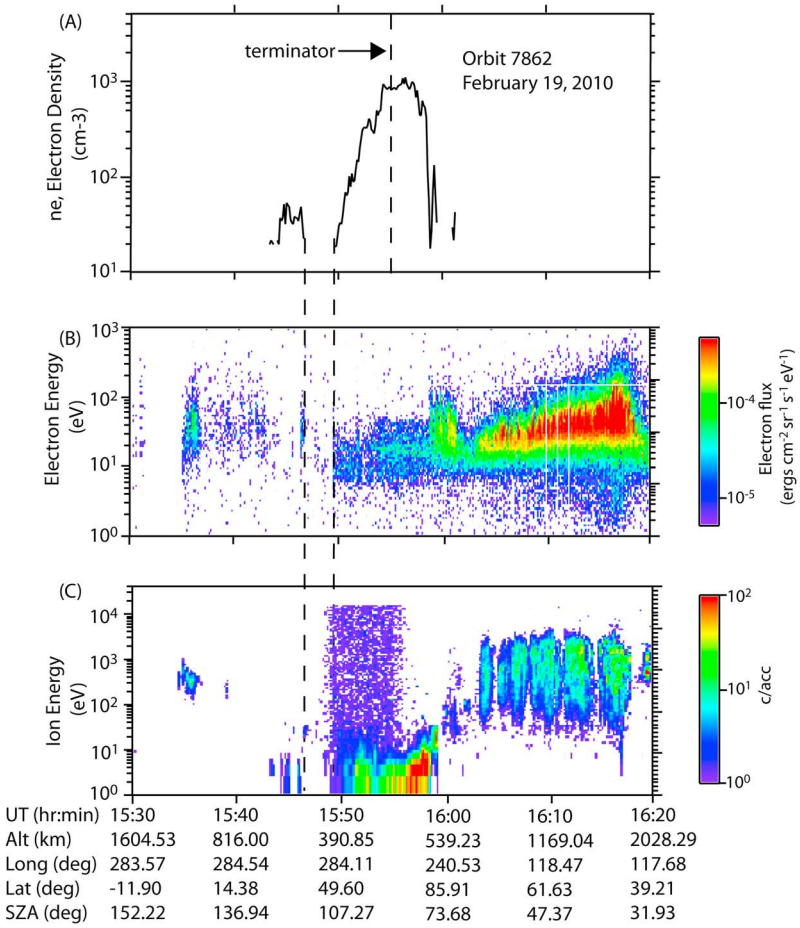


**Figure 10.** MEX data for the pass on 19 February 2010 (orbit 7862). (a) Local electron densities from MARSIS. A density depression is observed between about 1547 UT and 1550 UT. (b) Electron flux from ELS sector 9. At the time MARSIS density depression is seen, a depletion is observed in the electron flux, as well. The end of the depression corresponds to where the photoelectrons start to be dominant. (c) The ion flux from IMA sector 0. Any small intensity of low-energy ions are masked because of the ion light leak.

2110 UT, near parapsis. The depression is observed between 2058 UT and 2059 UT.

[27] Figures 9b and 9c show the ASPERA-3 ELS and IMA data, respectively, in a format similar to Figure 6. Again, the ELS is measuring over a narrower energy range every 1 s in this pass and the beginning of the photoelectrons is observed at 2103 UT. More electron flux is observed on the night side prior to 2103 UT, than after. In IMA data, there is an increase in the background just after this time, which is due to IMA's light leak. After the depression, the PPP observation becomes clearer in some ELS sectors, but no obvious PPP can be seen in sectors with oppositely directed pitch angles. This situation suggests that the depression occurs just before the field lines that contain the PPP. Again, the electron density depression, seen between 2058 UT and 2059 UT, seems to coincide with an increase in low-energy ion flux. In this case, the increase in ion energy seems to be due to spacecraft charging rather than ion flow. Even though the electron intensity does not change much during this event, the feature seems to exist in all IMA sectors with the same energy signature, but the ion intensities do vary around the IMA central measurement plane suggesting that IMA is measuring plasma at various pitch angles.

[28] Figure 10 provides the local electron densities from MARSIS, the electron flux from ELS and the ion flux from IMA, in the same format as Figure 6, but for the pass on 19 February 2010 (orbit 7862). The local electron densities start at about 1543:22 UT and continue up to 1546:46 UT, when an ionospheric depression starts. The depression ends at 1549:40 UT. At the times when MARSIS observes the depression, there is also a depletion in the ELS electron flux, which is the case for 11 other depressions we have studied. Investigation of different ELS sectors showed that the depletion in the electron flux is caused by a decrease in the electron flux to levels that fall below the instrument threshold. Some sectors have less flux than others, which seems to depend on pitch angles. Low levels of flux are unreliable and do not aid this analysis. Because of the ion light leak occurring during this time, any low intensity of low-energy ions are masked. The end of the depression corresponds to the location where the photoelectrons start to dominate. In almost half of the orbits, the depression is seen just before the PPP detection starts to dominate the electron

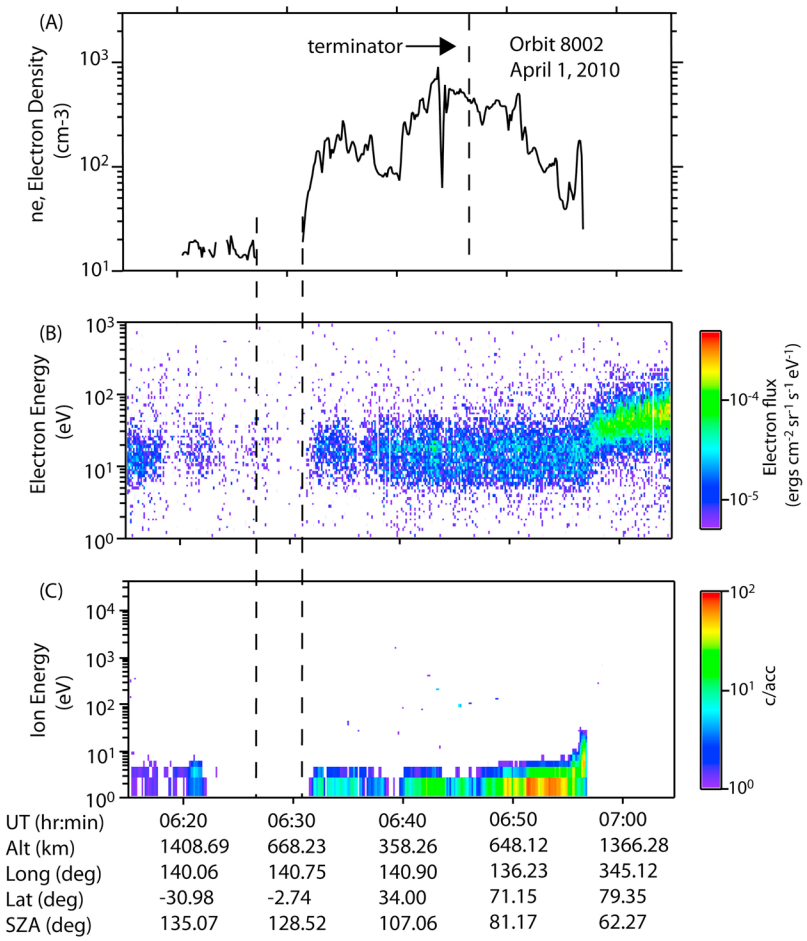


**Figure 11.** (a) MARSIS data, along with (b) ASPERA-3 ELS sector 9 and (c) IMA sector 0 are shown for a pass from 1 April 2010 (orbit 8002). The depression in local electron density data observed between 0627 UT and 0631 UT, looks more like a density gap and corresponds both to a decrease in the electron flux and loss of ion flux. The gap ends where the PPP starts.

data. Another example is the second depression in Figure 6, where the density depression is observed right before the steep density gradient at 0912:07 UT, which is at the start of PPP detection in the ELS data.

[29] In a few passes, such as the one shown in Figure 11, the density depression does not show the gradual decrease in density at the beginning of the structure. In Figure 11, the ASPERA-3 IMA and ELS data are shown together with MARSIS data for the pass from 1 April 2010 (orbit 8002) in the same format as in Figure 6. MARSIS obtains a local density, given by the solid black line in Figure 11a, beginning at 0620:29 UT when both electrons (Figure 11b) and ions (Figure 11c) are observed with ASPERA-3. The small drop in the MARSIS density between 0622:15 UT and 0622:45 UT and the small gap between 0623:30 UT and 0624:15 UT coincide with a loss of ion flux. At these times, no obviously related change in the electron flux is observed. The big depression in the local electron density observed between 0627 UT and 0631 UT corresponds both to a decrease in the electron flux and loss of ion flux. It is also worth noting that the depression ends where the PPP starts, as in Figures 6 and 10.

### 5.2. Size and Location

[30] At Venus, the depressions are large-scale structures with average east-west dimensions of about 1800 km [*Brace et al.*, 1983]. To calculate the width of a depression at Mars, such as the one shown in Figure 12, its size along the trajectory of the spacecraft (l in Figure 12) must be calculated. To do this, the time elapsed to cross the depression is multiplied by the speed of the spacecraft. It is assumed that the speed of the spacecraft does not change appreciably throughout the depression. Then, the altitude change throughout the depression, $a$, is calculated. The width of the depression is given by the Pythagorean theorem: $w^2 = l^2 - a^2$. The widths of the depressions vary between 340 km and 3280 km, with an average of 950 km. The results indicate that the depressions in the ionosphere of Mars are also large-scale structures similar to the size of the depressions at Venus. However, the shapes of the depressions in the ionosphere of Mars are more irregular than the depressions observed in the ionosphere of Venus. The electron density profiles at Venus show a smoother profile, with almost no fluctuations; and therefore, the depressions have smoother

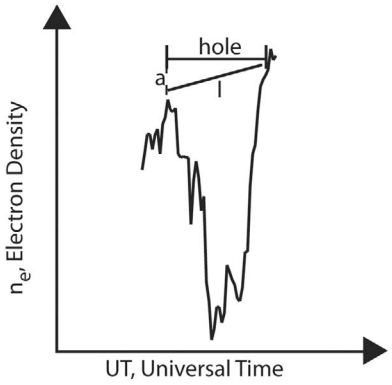


**Figure 12.** Example of an electron density depression. The width of a depression is given by the short horizontal line. Here, "l" is the size of the depression along the trajectory of the spacecraft and "a" is the altitude change through the depression.

shapes and they stand out more (for examples, see *Brace et al.* [1982]) than the depressions in the ionosphere of Mars.

[31] The locations of the individual depressions are also studied. In the Venus ionosphere, most of the depressions are observed in two latitude-local time zones [*Brace et al.*, 1982]. In the ionosphere of Mars, the depressions occur at all latitudes and longitudes; no obvious relationship exists between the occurrence of the depressions and their latitudes, longitudes, and local times. However, our data do not cover all SZAs and that may be the reason why the distribution of density depressions at Mars and Venus appear to be different. Figure 13 shows the altitude (*y* axis) and SZA (*x* axis) location of the depressions (squares), along with the data coverage (black dots). It should be noted that the depressions are spatially extended structures, and the SZA and altitude values in the middle of the depression are used in the figure. As Figure 13 shows, although the altitude of the depressions increases with increasing SZA, this is most probably an effect of the data coverage.

### 5.3. Discussion on Nightside Electron Density Depressions

[32] Nightside ionospheric density depressions in the ionosphere of Venus are widely observed structures and they are believed to be the site of significant plasma escape [*Brace et al.*, 1983]. The mechanism behind the existence of the depressions is explained as strong radial magnetic fields within the depressions, which prevent the entry of ions and electrons from the surrounding ionosphere. At the same time, plasma is removed from the region with either ion subsidence to the lower ionosphere, or ion loss to the magnetotail through electromagnetic processes [*Brace et al.*, 1982]. *Pérez-de-Tejada* [2004] concluded that the direction of the magnetic field with respect to the ecliptic plane can account for the ionospheric density holes at Venus.

[33] The electron density profiles of depressions observed at Mars are similar to those observed at Venus. We believe there are several reasons for the existence of the depressions in the ionosphere of Mars.

[34] Out of 66 passes, 21 of them displayed depressions, which correspond to 32%. A total of 27 density depressions are identified with MARSIS local electron density data, and 19 orbits are studied with the use of both MARSIS and ASPERA-3 (ELS and IMA) data. It is seen that in 12 cases, the low-energy ion flux increases. In 9 cases, the ion flux disappears completely or decreases. Also, the electron flux decreases in 19 depressions, and in four cases no change has been observed in the electron flux. It is seen that more than half of the density depressions in the MARSIS data correspond to the places where the PPP becomes dominant in the ASPERA-3 ELS data.

[35] This study of MARSIS and ASPERA-3 data suggests that different conditions are present for different depressions. The regions where the MARSIS density depression is observed, along with a decrease in the ASPERA-3 ELS and IMA data, could be places where the magnetic field is totally closed and no external plasma has access to these field lines. Therefore, sinks dominate sources, and the gradual recombination of ionized components leads to the depression in all three instruments. The partial screening of the nightside atmosphere of Mars by a weak intrinsic magnetic field of the planet was concluded by *Verigin et al.* [1991] to be one of the reasons for the variability of the Martian nightside atmosphere.

[36] Mars magnetic topology changes with the changes in the interplanetary magnetic field (IMF) and with the rotation of the planet. If a closed loop, which had been closed for enough time to lead to a depression, had sudden access to external plasma, it is possible that the electron and ion fluxes would be normal, while the MARSIS electron density would remain depressed.

[37] Another possibility for the cases where a depression in the ASPERA data is observed along with the depression in MARSIS electron densities is that the depressions in the electron flux are due to atmospheric degradation, where ASPERA-3 instrument dips below the Mars equivalent to the Earth's F region, into the dense neutral atmosphere.

[38] Density depressions that coincide with ion flow features in the IMA data, such as in Figure 8, are apparently similar to those seen at Venus. Plasma escape from the ionosphere to the magnetosheath can cause density depressions. This process may involve waves or instabilities at the

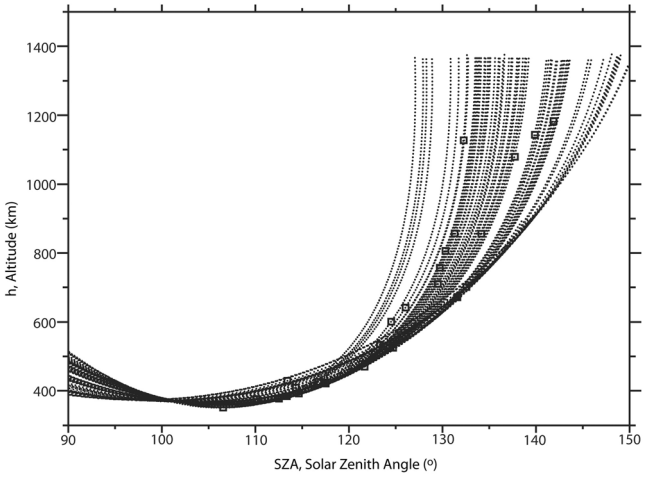


**Figure 13.** The altitude (*y* axis) and SZA (*x* axis) location of the middle point of the density depressions (squares), along with the data coverage (black dots).

boundary between the ionosphere and magnetosheath, or it may be the effect of a radially directed magnetic field, such as in the ionosphere of Venus. Unfortunately, since Mars Express does not carry a magnetometer, we are unable to measure the direction of the magnetic field. However, we do know that ion energy drifting up and then back down, such as in Figure 8, or ions gradually increasing their energy from about 10 eV as they transition to magnetosheath energies, as in Figure 8, are signatures of ion flow. In both cases, the ions are escaping and being accelerated away from the planet. Also, ion velocity seems to exceed the MARSIS flow velocity limit [*Duru et al.*, 2010] at the ion energy apex.

[39] As stated earlier, in many cases, the density depressions are observed adjacent to the end of the PPP. In some cases, the abrupt end of these dayside atmospheric photoelectrons cannot be due to loss of UV flux, since PPP occurs well past the local terminator. It is very probable that those places are the boundaries between the closed and open magnetic field lines. Since the photoelectrons are from the dayside, either the magnetic field lines arch over the terminator, or are draped to the nightside. A magnetic pressure bump at the boundary, assuming the total pressure is constant, can cause the electron density to decrease. Examination of some Mars Global Surveyor (MGS) orbits with similar shape to some of the MEX orbits, but with a different local time, showed a peak in the magnetic field, which supports this explanation [*Mitchell et al.*, 2001].

[40] At Venus, plasma clouds and streamers are observed above the ionopause. They are thought to be the results of ionospheric plasma removal processes by the solar wind [*Brace et al.*, 1983]. It is very probable that similar structures exist also in the ionosphere of Mars. *Gurnett et al.* [2010] showed that the power spectrum of electron density fluctuations is consistent with a Kolmogorov spectrum, and instabilities or solar wind pressure perturbations could create the turbulence. This turbulence can easily cause plasma removal or streamers above the ionopause, similar to the ones encountered in the ionosphere of Venus. These structures can explain some of the depressions, especially the ones that are at high altitude. It is possible that the spacecraft travels first through the clouds or streamers with ionospheric plasma, then for the duration of the depression it may be immersed in solar wind plasma, after which it may enter the ionosphere where the density increases as the spacecraft altitude decreases.

[41] The density depressions at Mars are more irregular than the holes encountered in the ionosphere of Venus, which are believed to reoccur at particular local times and latitudes. At Mars, it is not possible to talk of one type of depression that shows the same features for all cases. However, it is possible to categorize the depressions according the behavior of the ASPERA-3 data.

[42] One should be aware that, with both MARSIS and ASPERA-3 (ELS and IMA), each instrument has its threshold. By using the term "depression," we mean that the signal in the detector lies below its threshold. Thus, there could be density below the MARSIS threshold or flux below the ELS or IMA thresholds that the instrument cannot detect. In addition, both ELS and IMA have further restrictions in that they are measuring plasma from a space that is not three-dimensional. This is more of a restriction on the low-energy ions that are collimated into a flow direction. Because of their direction, it is possible that flowing ions may not be detected if the flow is too far outside the field of view of IMA.

[43] It is worth keeping in mind, while analyzing the altitude profiles, that special conditions apply to the physics that plays an important role within the terminator region. The terminator is the region defined at the optical surface of the planet for SZA = 90°. However, the border between sunlit and dark plasma is located at the height $h = R_m(1/\mathrm{Cos}(SZA) - 1)$. On the Sun side of the terminator, the plasma is in sunlight, and on the other side of the terminator, the plasma is in darkness. However, a penumbra, which is altitude dependent, is present between daylight and complete darkness. As the terminator is crossed by a spacecraft from daylight into darkness, part of the atmosphere becomes affected by the sunlight and part by the umbra. The proportions of the affected altitude profile are dependent on the spacecraft path. For the case on the MEX spacecraft, the altitude profiles of plasma are bathed in a varying amount of light. This situation is even more complicated since the atmosphere around Mars is opaque to various radiation wavelengths at different altitudes. Thus, the planet presents a different size obstacle to different wavelengths, which leads to an altitude dependency in the excitation wavelength for plasma as well.

[44] Another important factor at Mars is the presence of crustal magnetic fields that form minimagnetospheres. When these regions are in daylight, they can trap plasma as the plasma bounces between the ends of the magnetic bubble. As the planet rotates and encounters the terminator region, part of the magnetic bubble often exists in daylight and part stretches across the terminator into darkness [*Brain et al.*, 2010; *Frahm et al.*, 2008; *Kallio et al.*, 2008]. This can cause the plasma in the daylit region to be production dominated, while the plasma in the region in darkness is destruction dominated. As the minimagnetosphere rotates through the terminator region, the ratio between creation and destruction mechanisms varies. In the region of the terminator, the crustal planetary magnetic field is transitioning from a nighttime configuration to a daytime configuration. The exact configuration is dependent on the interplanetary magnetic field strength and its direction.

[45] Finally, it would be misleading to suggest that the depressions in the electron density profiles are only observed on the nightside. Similar structures are also seen on the dayside. However, they are observed less frequently, and we believe that they are caused by different mechanisms and for different reasons.

## 6. Summary

[46] The nightside ionosphere of Mars has not been studied as well as the dayside has. Here, we provide some insights into the nightside from local electron densities obtained from the electron plasma oscillations as measured by MARSIS. The first feature that is observed is the high variability of the nightside ionosphere. The electron density profiles display large fluctuations.

[47] When compared with the dayside, the electron density values are lower (about a factor of 3 at around 400 km). We have shown in Figure 4 that the median electron density is about 300 $cm^{-3}$ at around 400 km and that it decreases to

about 20 $cm^{-3}$ at around 1200 km. Also, the exponential relationship between the median electron density and the altitude is evident from this plot. The median electron density as a function of SZA is also studied. We have shown that the electron density at the altitudes, where local measurements are obtained, does not change much with changing SZA, as was also the case on the dayside.

[48] Steep electron density gradients are accepted and commonly observed in Venus as an ionopause boundary. At Mars, similar steep density gradients, which have been interpreted as transient ionopauses, are sometimes observed on the dayside. This study provides the first indication of the sharp density gradients on the nightside. These cases are observed in only 15% of the total sample, suggesting that they are transient cases. They are mostly observed where the photoelectrons become dominant in the ASPERA-3 ELS data.

[49] Another structure encountered in the nightside ionosphere of Mars is electron density depressions, which are defined as deep troughs in the electron density. Nightside electron density holes were previously observed at Venus, generally in a particular latitude-local time region, at the places where the magnetic field is almost vertical. At Mars, they are observed at all latitudes and longitudes, and exhibit no consistent pattern in local time. It is worth mentioning that, although there are many similarities between the upper atmospheres and ionospheres of Venus and Mars, Mars possesses crustal magnetic fields while Venus does not. This can account for some of the differences.

[50] As at Venus, the electron density holes are large structures with widths varying between 340 and 3280 km. Study of the ASPERA-3 ELS and IMA data showed that, in some cases, the depressions in the MARSIS data correspond to depletion regions in the ASPERA-3 data while, in other cases, ion flow features are observed. In more than half of the cases, electron density depressions are observed at the end of the PPP. It is concluded that different processes, such as plasma escape along radial magnetic field lines or due to instabilities, recombination of ionized components at the locations with totally closed magnetic field lines, and atmospheric degradation, could cause the depressions.

[51] **Acknowledgments.** Research at the University of Iowa was funded by contract 1224107 with the Jet Propulsion Laboratory, and NASA contract NASW-00003 at Southwest Research Institute.

[52] Masaki Fujimoto thanks the reviewers for their assistance in evaluating this paper.

## References

Barabash, S., et al. (2004), ASPERA-3: Analyzer of space plasmas and energetic ions for Mars Express, in *Mars Express: The Scientific Payload*, edited by A. Wilson, *Eur. Space Agency Spec. Publ.*, *ESA SP-1240*, 121–139.

Barabash, S., et al. (2007), The Analyzer of Space Plasmas and Energetic Atoms (ASPERA-3) for the Mars Express Mission, *Space Sci. Rev.*, *126*, 113–164, doi:10.1007/s11214-006-9124-8.

Brace, L. H., R. F. Theis, H. G. Mayr, S. A. Curtis, and J. G. Luhmann (1982), Holes in the nightside ionopshere of Venus, *J. Geophys. Res.*, *87*(A1), 199–211, doi:10.1029/JA087iA01p00199.

Brace, L. H., H. A. Taylor, T. I. Gombosi, A. J. Kliore, W. C. Knudsen, and A. F. Nagy (1983), The ionosphere of Venus: Observations and their interpretation, in *Venus*, edited by D. M. Hunten et al., pp. 779–840, Univ. of Ariz. Press, Tucson.

Brain, D. A., A. H. Baker, J. Briggs, J. P. Eastwood, J. S. Halekas, and T.-D. Phan (2010), Episodic detachment of Martian crustal magnetic fields leading to bulk atmospheric plasma escape, *Geophys. Res. Lett.*, *37*, L14108, doi:10.1029/2010GL043916.

Chicarro, A., P. Martin, and R. Traunter (2004), Mars Express: A European mission to the red planet, in *Mars Express: The Scientific Payload*, edited by A. Wilson, *Eur. Space Agency Spec. Publ.*, *ESA SP-1240*, 3–16.

Duru, F., D. A. Gurnett, D. D. Morgan, R. Modolo, A. Nagy, and D. Najib (2008), Electron densities in the upper ionosphere of Mars from the excitation of electron plasma oscillations, *J. Geophys. Res.*, *113*, A07302, doi:10.1029/2008JA013073.

Duru, F., D. A. Gurnett, R. A. Frahm, J. D. Winningham, D. D. Morgan, and G. G. Howes (2009), Steep, transient density gradients in the Martian ionosphere similar to the ionopause at Venus, *J. Geophys. Res.*, *114*, A12310, doi:10.1029/2009JA014711.

Duru, F., D. A. Gurnett, J. D. Winningham, R. A. Frahm, and R. Modolo (2010), A plasma flow velocity boundary at Mars from the disappearance of electron plasma oscillations, *Icarus*, *206*, 74–82, doi:10.1016/j.icarus.2009.04.012.

Fox, J. L., and J. F. Brannon (1993), Upper limits to the nightside ionosphere of Mars, *Geophys. Res. Lett.*, *20*(13), 1339–1342, doi:10.1029/93GL01349.

Frahm, R. A., et al. (2006), Location of atmospheric photoelectron energy peaks within the Mars environment, *Space Sci. Rev.*, *126*, 389–402, doi:10.1007/s11214-006-9119-5.

Frahm, R. A., E. Kallio, Y. Futaana, A. Fedorov, and P. Janhunen (2008), Variations of the magnetic field near Mars caused by magnetic crustal anomalies, *Planet. Space Sci.*, *56*(6), 856–860, doi:10.1016/j.pss.2007.12.018.

Frahm, R. A., et al. (2010), Estimation of the escape of photoelectrons from Mars in 2004 liberated by the ionization of carbon dioxide and atomic oxygen, *Icarus*, *206*, 50–63, doi:10.1016/j.icarus.2009.03.024.

Gurnett, D. A., and A. Bhattacharjee (2005), *Introduction to Plasma Physics with Space and Laboratory Application*, 91 pp., Cambridge Univ. Press, Cambridge, U. K.

Gurnett, D. A., et al. (2005), Radar soundings of the ionosphere of Mars, *Science*, *310*, 1929–1933, doi:10.1126/science.1121868.

Gurnett, D. A., D. D. Morgan, F. Duru, F. Akalin, J. D. Winningham, R. A. Frahm, E. Dubinin, and S. Barabash (2010), Large density fluctuations in the Martian ionospehere as observed by the Mars Express radar sounder, *Icarus*, *206*, 83–94, doi:10.1016/j.icarus.2009.02.019.

Haider, S. A., J. Kim, A. F. Nagy, C. N. Keller, M. I. Verigin, K. I. Gringauz, N. M. Shutte, K. Szego, and P. Kiraly (1992), Calculated ionization rates, ion rates, ion densities, and airglow emission rates due to precipitating electrons in the nightside ionosphere of Mars, *J. Geophys. Res.*, *97*(A7), 10,637–10,641, doi:10.1029/92JA00317.

Kallio, E., R. A. Frahm, Y. Futaana, A. Fedorov, and P. Janhunen (2008), Morphology of the magnetic field near Mars and the role of the magnetic crustal anomalies: Dayside region, *Planet. Space Sci.*, *56*(6), 852–855, doi:10.1016/j.pss.2007.12.002.

Lillis, R. J., M. O. Fillingim, L. M. Peticolas, D. A. Brain, R. P. Lin, and S. W. Bougher (2009), Nightside ionosphere of Mars: Modeling the effects of crustal magnetic fields and electron pitch angle distributions on electron impact ionization, *J. Geophys. Res.*, *114*, E11009, doi:10.1029/2009JE003379.

Mitchell, D. L., M. H. Acuña, and J. E. P. Connerney (2001), MGS Mars/Moons MAG/ER Pre-map ER Omnidirectional Flux V1.0 (PDS), http://nssdc.gsfc.nasa.gov/nmc/datasetDisplay.do?id=PSFP-00285, NASA Natl. Space Sci., Greenbelt, Md.

Němec, F., D. D. Morgan, D. A. Gurnett, and F. Duru (2010), Nightside ionosphere of Mars: Radar soundings by Mars Express spacecraft, *J. Geophys. Res.*, *115*, E12009, doi:10.1029/2010JE003663.

Němec, F., D. D. Morgan, D. A. Gurnett, and D. A. Brain (2011), Areas of enhanced ionization in the deep nightside ionosphere of Mars, *J. Geophys. Res.*, *116*, E06006, doi:10.1029/2011JE003804.

Pérez-de-Tejada, H. (2001), Solar wind erosion of the Venus polar ionosphere, *J. Geophys. Res.*, *106*(A1), 211–219, doi:10.1029/1999JA000231.

Pérez-de-Tejada, H. (2004), Plasma channels and electron density profiles near the midnight plane in the Venus nightside ionosphere, *J. Geophys. Res.*, *109*, A04106, doi:10.1029/2002JA009811.

Picardi, G., et al. (2004), MARSIS: Advanced radar for subsurface and ionosphere sounding, in *Mars Express: A European Mission to the Red Planet*, *Eur. Space Agency Spec. Publ.*, *ESA SP-1240*, 51–70.

Safaeinili, A., W. Kofman, J. Mouginot, Y. Gim, A. Herique, A. B. Ivanov, J. J. Plaut, and G. Picardi (2007), Estimation of the total electron content of the Martian ionosphere using radar sounder surface echoes, *Geophys. Res. Lett.*, *34*, L23204, doi:10.1029/2007GL032154.

Schunk, R. W., and A. F. Nagy (2009), *Ionospheres: Physics, Plasma Physics, and Chemistry*, Cambridge Univ. Press, Cambridge, U. K., doi:10.1017/CBO9780511635342.

Verigin, M. I., K. I. Gringauz, N. M. Shutte, S. A. Haider, K. Szego, P. Kiraly, A. F. Nagy, and T. I. Gombosi (1991), On the possible source of the ionization in the nighttime Martian ionosphere: 1. PHOBOS 2 HARP electron spectrometer measurements, *J. Geophys. Res.*, *96*(A11), 19,307–19,313, doi:10.1029/91JA00924.

Zhang, M. G. H., J. G. Luhmann, and A. J. Kliore (1990), An observational study of the nightside ionosphere of Mars and Venus with radio occultation methods, *J. Geophys. Res.*, *95*(A10), 17,095–17,102, doi:10.1029/JA095iA10p17095.

F. Duru, D. A. Gurnett, and D. D. Morgan, Department of Physics and Astronomy, University of Iowa, Iowa City, IA 52242, USA. (firdevs-duru@uiowa.edu)

R. A. Frahm and J. D. Winningham, Southwest Research Institute, PO Box 28510, San Antonio, TX 78228, USA.

A. F. Nagy, Department of Atmospheric, Oceanic and Space Sciences, University of Michigan, Ann Arbor, MI 48109, USA.